

Volumetric velocimetry of the particle motion induced by surface acoustic waves

Jörg König¹, Florian Kiebert¹, Hagen Schmidt¹ and Carsten Kykal²

¹ SAWLab Saxony, IFW Dresden, P.O. 270116, 01171 Dresden, Germany
J.Koenig@ifw-dresden.de

² TSI GmbH, Neuköllner Str. 4, 52068 Aachen, Germany

ABSTRACT

The use of surface acoustic waves (SAW) allows for fluid and micro particle manipulation by exploiting either the acoustic streaming or the acoustic radiation force. However, detailed knowledge about both phenomena is still missing, regarding not only the three-dimensional acoustic excitation, but also the interaction between fluid and particle depending on their physical properties. For the first time, defocus digital particle image velocimetry (DDPIV) was applied to volumetrically measure the particle motion induced by a SAW-device immersed in a fluid. This measurement technique meets the general requirements for observing the three-dimensional acoustic excitation of particle motion, by delivering high spatial resolution (down to 0.06 mm^3) despite a comparably large measurement volume (40 ml). Several experiments were carried out using various viscous fluids and different kinds of particles of different size. It is shown that the acoustic streaming-effect dominates the particle motion, which is induced by an SAW-field of finite size ($\approx 2 \text{ mm} \times 4.8 \text{ mm}$) at a $90 \mu\text{m}$ wavelength. In contrast to previous publications, the acoustic radiation force can be neglected, even though particle size exceeds a critical value. The three-dimensional behavior of the fluid motion is characterized by two narrow jets propagating bi-directionally through the fluid, depending on the fluid's viscosity. While both jets deeply penetrates into pure water with high velocity (80 mm/s at maximum), high viscous fluids limit the acoustically-induced fluid motion to the immediate vicinity of the SAW-device. In case of a highly viscous fluid, natural convection evolves near the SAW-device due to a local temperature increase, since most of the acoustic energy dissipated into heat.

1. INTRODUCTION

Active mixing of small fluid volumes is of great importance for numerous applications, e.g. in chemistry, biology or medicine. At many analytical methods, however, low Reynolds numbers exist that make it difficult to mix fluids within short time, since mixing is governed by diffusion. Therefore, several approaches have been investigated to speed up mixing by applying external forces, e.g. thermal, electrical or magnetic [7]. In recent years, ultrasonic pressure waves induced by surface acoustic waves (SAWs) have attracted researchers' attention in order to mix small amounts of liquids or to separate micro particles inside microchannels, either by exploiting the acoustic radiation force or the acoustic streaming [4]. The large frequency range of SAWs, typically between 10 MHz to 1 GHz, enables fast adaptation to the physical dimensions of the application. In that way, SAWs provide an effective means to mix fluids not only in lab-on-a-chip devices, but also in systems of somewhat larger scale, e.g. in a test tube of an autosampler. At this particular application, rapid mixing is usually achieved by employing a magnetic stirrer that spin small fleas inside the test tube. However, the insertion and the removal of the small fleas is very time consuming. A promising alternative is the use of a mixer based on SAWs that mixes the reacting solution within short time just before the sampling.

In figure 1(a) the active part of a mixer utilizing SAWs is depicted. The mixer is made of a transparent piezoelectric substrate (128° YX Lithium Niobate, LiNbO_3) fixed on a PCB board for electrical connection. On its surface thin-film (300 nm thickness) interdigitated electrodes of aluminum are deposited, the so-called interdigital transducer (IDT). The width of the electrodes as well as their distance to each other amount to a quarter of the wavelength λ of the SAW, which is determined by the geometrical periodicity of the IDT. By applying an electric field with high frequency, $f = c_{\text{saw}}/\lambda$, corresponding to the velocity c_{saw} and the wavelength λ of the SAW, the inverse piezoelectric effect generates elastic deformations of the substrate's surface, so that an SAW disseminates bi-directionally along the crystallographic X -axis of the chip. The typical transverse amplitude of the SAW amounts to less than 10 nm depending on the electrical power P_{el} applied to the IDT. Once

in contact with a liquid, the liquid's viscosity causes part of the SAW to refract into the liquid as a bulk acoustic wave (BAW) whilst the SAW is proportionally damped, as schematically depicted in figure 1(b). The refraction angle Θ , usually referred as Rayleigh angle, depends on the acoustic velocity of the SAW, c_{SAW} , and the fluid c_{fluid} . The refracted acoustic wave induces laminar fluid flow due to the attenuation of acoustic energy within the liquid [8]. This phenomenon is called acoustic streaming. The streaming pattern corresponds to the propagation and the intensity distribution of the BAW that is of three-dimensional character given by a finite size of excitation (width and length of the damped SAW), acoustic power, refraction and attenuation. Thus, the resulting fluid flow is necessarily complex and very difficult to describe.

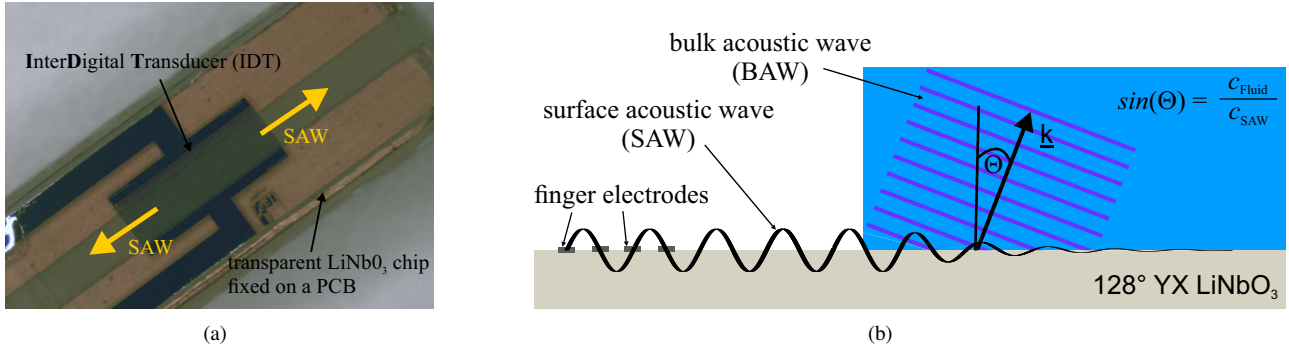


Figure 1: (a) top view of the active part of an SAW-mixer and (b) principle of the acoustic streaming: fluid motion is induced along the propagation direction of the bulk acoustic wave.

For better understanding the acoustic streaming arising from SAWs fluid flow measurements are of vital importance. Following the simplified model depicted in figure 1(b), first flow measurements were carried out using planar particle image velocimetry (PIV) in order to study the dependence of the acoustic streaming on frequency and power [2]. The measurements were compared with simulations, assuming a certain damping of the SAW at the interface between fluid and piezoelectric substrate. Although, very high frequencies (up to 1 GHz) were applied, the influence of the acoustic radiation force on particle velocity was not considered in detail. However, this force has to be borne in mind when measuring the acoustically induced fluid motion using a particle based measurement technique like PIV, since high systematic uncertainties can occur due to the superimposed particle motion originating from the influence of the acoustic radiation force. In addition, the simplified two-dimensional model does not represent real application of SAWs to induce fluid motion, since neither a wall of a microchannel nor the actual position of an SAW-mixer inside a test tube is considered. The latter means, not only a part of the piezoelectric substrate is in contact with the fluid, as illustrated in figure 1(b), but also the IDT. In that more practical case, the IDT is electrically and mechanically loaded by the fluid, causing a much more complex generation and propagation of the SAW that is difficult to approximate with a two-dimensional model. In order to gain first experimental insight into the fluid motion induced by an SAW-mixer immersed in the fluid, flow measurements were carried out using the volumetric three-component velocimetry (V3V) from TSI Inc. This measurement technique offers very low spatial uncertainty of particle position, e.g. down to $30 \mu\text{m}$ in depth, despite a comparably large measurement volume, allowing effectively analyzing the three-dimensional character of the acoustic radiation- and streaming induced particle motion within the entire region of interest, i.e. within the attenuation length of the BAW (up to 40 mm in the present experiments). As the resulting three-dimensional particle motion depends not only on the acoustic characteristics (frequency, acoustic power), but also on the properties of the fluid (density, viscosity, speed of sound) and the particle (density, size), various experiments were carried out using different kinds of fluids and particles.

2. EXPERIMENTAL SETUP

Figure 2 illustrates the setup used to measure the acoustically-induced particle motion originating from surface acoustic waves. It consists of a cuvette (manufacturer Hellma Analytics) made of glass with optical quality and inner dimensions of $H \times W \times D = 50 \text{ mm} \times 50 \text{ mm} \times 20 \text{ mm}$. To ensure no-slip condition at each wall the cuvette is closed with a glass slid. The LiNbO_3 -chip with the IDT is immersed in the fluid at the right hand-side of the glass cuvette. Its crystallographic X -axis corresponds y -axis of the experimental setup. The height position of the IDT is about the half of the cuvette height $H/2$. In that way, the distance to glass walls is maximized. For the present setup, an IDT at a $\lambda = 90 \mu\text{m}$ wavelength (corresponding to $f \approx 44.4 \text{ MHz}$) was used. Its number of interdigital electrode pairs amounted to 30, yielding a total length (y -direction) of the IDT of about 2.7 mm. Its aperture, which corresponds to the z -direction, amounted to 2 mm.

According to the expected radiation characteristic of the IDT, the bulk acoustic wave primarily propagates along the xy -plane of the experimental setup. Following [8], the attenuation length α of the BAW in the fluid reads

$$\alpha = \frac{3}{4} \frac{c_{\text{fluid}}^2}{(2\pi \cdot f)^2} \cdot \frac{\rho}{\eta}, \quad (1)$$

and can be estimated depending on the frequency of the sound wave f , the speed of sound c_{fluid} , viscosity η and density ρ of the fluid.

Three different working fluids were used: de-ionized water and a mixture of water and glycerin by weight percentages either of 50%, 50% or 25%, 75%. The attenuation length α , the density ρ , the viscosity η and the speed of sound c_{fluid} of each fluid are listed in table 1. As appears from table 1, the higher the amount of glycerin and, therefore, the higher the viscosity of the fluid the shorter the attenuation length of the BAW. Hence, the acoustically induced particle motion is spatially confined depending on the fluid's viscosity. The maximum attenuation length amounts to 35.9 mm, which is smaller than the maximum possible length of particle motion given by the width W of the glass cuvette in conjunction with a radiation of the BAW at the Rayleigh angle. Hence, the particle motion can be considered to be unaffected by the limited size of the glass cuvette.

	fluid 1	fluid 2	fluid 3
	de-ionized water	mixture of water/glycerin (50/50)	mixture of water/glycerin (25/75)
ρ [kg m ⁻³] [*]	997	1127	1192
η [mPa s] [*]	0.9	5.0	27.7
c_{fluid} [m s ⁻¹] ⁺	1497	1729	1839
α [mm]	35.9	11.2	2.6

^{*} estimated following Cheng [1]

⁺ according to Fergusson [5]

Table 1: Overview about the fluids used in the experiments.

Taking the maximum attenuation length into account, a measurement technique has to be applied that enables the observation of the acoustic radiation- and streaming-induced particle motion not only within this entire region of interest, but also with sufficient spatial resolution regarding the aperture of the IDT of 2 mm in size. To fulfill these requirements the volumetric three-component velocimetry (V3V) from TSI Inc. was applied. This measurement technique bases on the defocused digital particle image velocimetry (DDPIV), which has been introduced by Willert et al., see [12]. Instead of a single-camera system utilizing a three-pinhole mask, an optical system composed of three individual cameras (Powerview 4MP CCD-camera) arranged in a triangular configuration, as described by Pereira et al., see [9], was used to acquire the three-dimensional three-component (3D3C) particle motion inside the glass cuvette. The alignment of the optical system to the glass cuvette is schematically depicted in figure 2. The optical axis of the V3V is orthogonally aligned to the glass wall of the cuvette. Camera lenses with a focal length of 50 mm and a small f-number of $f/16$ were used to get sharp images of all particles inside the entire glass cuvette. In order to capture two sets of three particle images, which compose the virtual image plane of the V3V, an Nd:YAG dual cavity laser (Evergreen 200 mJ, Quantel) with well-known time interval Δt between the double pulses was used to illuminate the particles from the side. To get nearly homogeneous illumination with high intensity over the entire glass cuvette, two cylindrical lenses with perpendicular orientation were used to conically span the laser light. The time difference Δt between the pulses was adjusted prior to each measurement. In that way, particle images suitable for particle tracking could be obtained for each individual parameter set, e.g. the electrical power P_{el} applied to the IDT. For each measurement, 200×2 recordings of triple-images were acquired at a repetition rate of 15 Hz. At each time of image capture ($t_0, t_0 + \Delta t$), particles were identified inside the virtual image plane via their corresponding triplet-image, according to the principle of the DDPIV, where the centroid and the size of the triplet determine the in-plane- (x, y) and the depth-position (z), respectively. To track the particles in 3D from the first image capture, at time t_0 , to the second, at time $t_0 + \Delta t$, the relaxation method was applied. The relation between 3D particle position and triplet image was calibrated prior to the measurements using a calibration target equipped with artificial particles, at well-known depth-positions inside the glass cuvette. According to the calibration result, the uncertainty of the particle position can be less than 30 μm in depth. Therefore, particles can be precisely tracked in 3D, despite a comparably large measurement volume of ca. 50 mm \times 50 mm \times 16 mm in size. For further evaluation, the randomly distributed velocity vectors were ensemble-averaged and interpolated onto a rectangular grid using Gaussian-weighted interpolation based on vector distance from the grid nodes. The minimum voxel size for interpolation amounted to 2 mm \times 1 mm \times 1 mm. The overlapping between neighboring voxels amounted to 70% at maximum, yielding a minimum regular grid spacing of 0.3 mm. Hence, the acoustically-induced particle motion could be analyzed with high spatial

resolution of about 0.06 mm^3 inside the measurement volume, containing up to 653000 velocity vectors. The measurement results will be discussed in the next section.

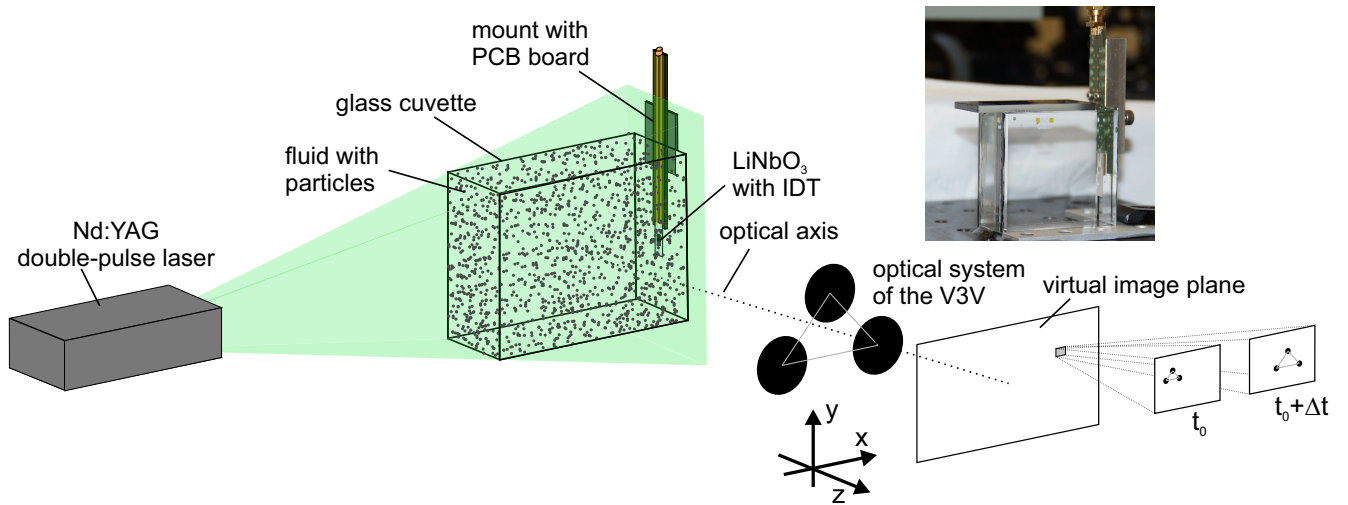


Figure 2: Sketch of the experimental setup. The photo shows the glass cuvette with the SAW-mixer immersed in the fluid.

3. MEASUREMENT RESULTS

3.1 General behavior of particle motion

At first, the general structure of particle motion induced by surface acoustic waves inside the glass cuvette will be discussed. For this, the measurement result of hollow glass spheres suspended in de-ionized water is exemplary depicted in figure 3(a). The diameter of the hollow glass spheres ranged from $8 \mu\text{m}$ to $12 \mu\text{m}$. Their mean density, 1.1 g/cm^3 , almost matches that of the water. For the measurement example depicted in figure 3(a), the electrical power applied to the IDT amounted to $P_{el} = 250 \text{ mW}$. The green iso-surfaces represent areas with a velocity magnitude of 15 mm/s . As can be clearly identified,

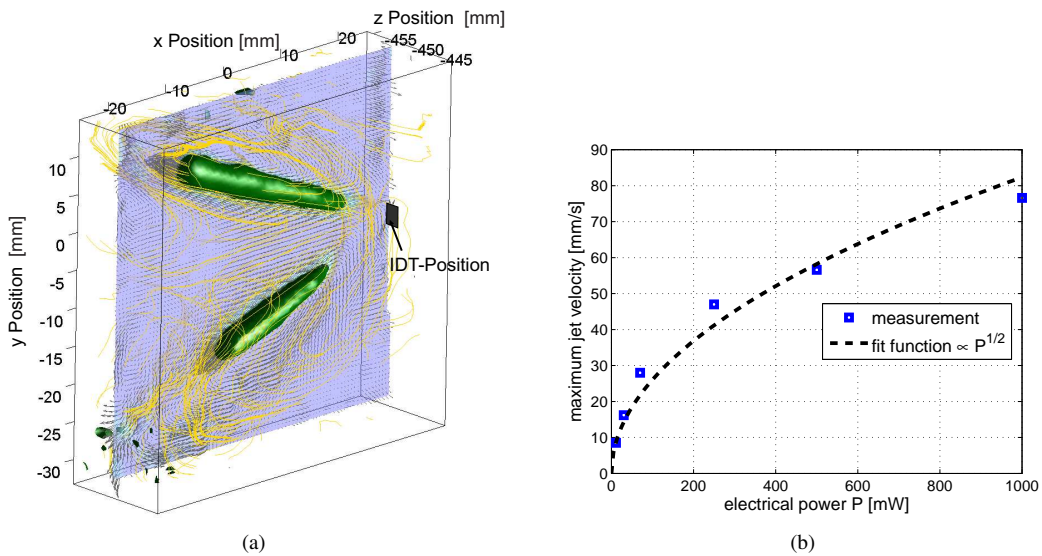


Figure 3: (a) 3D measurement result of the acoustically-induced particle motion in water at an electrical power of $P_{el} = 250 \text{ mW}$. The green isosurfaces represent areas with a velocity magnitude of 15 mm/s . (b) measured maximum jet velocity vs. electrical power P_{el}

the bi-directional acoustic excitation of the SAW causes two narrow jets of particle motion that primarily propagate in

xy-direction. The semi-angle of 20.6° in between the two jets nearly coincides to the theoretical Rayleigh angle, which amounts to approximately 22° at a water temperature of about 25°C . As can be seen in figure 4(a), the maximum velocity of both jets is quite similar, whereas their penetration depths slightly differ from each other. The reason for this non-symmetrical behavior, which is independent of the electrical power applied, is still unknown and needs further investigations.

Measurements at six different power levels, ranging from 10 mW to 1 W, were conducted. To accurately adjust the electrical power a commercial 'Power SAW Generator' (manufacturer BelektroniG GmbH) was used. According to the scattering parameter s_{11} , simultaneously acquired by the 'Power SAW Generator', almost 70% of the electrical power applied to the IDT dissipated into the fluid. For each measurement, the measurement data were processed with the INSIGHT-4G software from TSI Inc. following the processing scheme mentioned above. Afterwards, the averaged and interpolated velocity vectors were imported in Matlab. For further evaluation, a transformation of the velocity vectors was performed, taking the radiation angle of the BAW, which is given by the Rayleigh angle, into account. By doing this, the particle velocity in axial direction of the jets coincides with the radiation of the BAW. For further usage, this velocity is called jet velocity v_j . In addition, the characteristics of the jets were determined by iteratively fitting a two-dimensional Gaussian function to the velocity data at each x -position. In that way, jet velocity v_j , width and central position of the jets can be analyzed, in detail, at each axial-position (taking the Rayleigh angle into account). With a minimum width of 2 mm in z - and 4.4 mm in y -direction, corresponding to the excitation size of the SAW given by the aperture of the IDT and the damping of the SAW, the jets diverge up to 10 mm at maximum, depending on the electrical power applied. Interestingly, the higher the electrical power P_{el} applied the more spatially confined the jets. For more details about the jet characteristics in water, we refer to [6]. Furthermore, the measured maximum jet velocity obviously scales with $\propto P^{1/2}$, see figure 3(b), which is in good agreement to the predictions of a turbulent jet model [8] and a laminar jet model at high electrical power [2].

3.2 Influence of particle size

As briefly mentioned in the introduction, the particle velocity can be affected not only by the acoustic streaming, but also by the acoustic radiation force. Their influence depends on the experimental conditions, e.g. the ratio between size of the particle and wavelength of the bulk acoustic wave (BAW). For instance, Skowronek et al. used the dimensionless number $\kappa = k \cdot d/2$, depending on the wavenumber k of the BAW and particle diameter d , to illustrate the influence of the acoustic radiation force acting on polystyrene particles suspended in deionized water [11]. Based on measurement results, they found a critical value $\kappa_{crit} = 1.2$ at which particles start to be deflected inside a microchannel due to the influence of acoustic radiation force. Below this critical value acoustic streaming dominates. Destgeer et al. confirmed this result and found $\kappa = 1.4$ at which particles experienced maximum acoustic radiation force [3]. Again, the influence of the acoustic radiation force vanishes for particle sizes yielding $\kappa < 1$ [3]. Considering the frequency of the acoustic wave used in the present experiments, a particle suspended in water should have a diameter of less than $10.7\ \mu\text{m}$ ($\kappa = 1$). However, very small particles may produce particle images of poor quality, since very small numerical apertures are necessary to span the measurement volume in depth at macroscopic DDPIV. Besides an optimization of the experimental setup, measurements utilizing various particle sizes were conducted in order to determine the minimum particle diameter to be used.

According to Settnes et al., the acoustic radiation force acts on particles, proportional to $\propto d^2$, if density of the fluid and particle do not match [10]. It applies: the higher the mismatch of density the higher the acoustic radiation force [10]. For that reason, silver-coated polystyrene particles were applied, whose density, $2.4\ \text{g/cm}^3$, significantly differ from that of water and produce particle images of sufficient quality even at small size. To distinguish between $\kappa < 1$, $\kappa \approx 1$ and $\kappa > 1$, three different particles of $3.5\ \mu\text{m}$, $11\ \mu\text{m}$ and $21\ \mu\text{m}$ in diameter were used for velocity measurements under same experimental conditions (fluid: water, $P_{el} = 105\ \text{mW}$). Thus, the resulting particle velocity might alter depending on κ . However, while higher velocities with increasing diameter might be expected, the values in table 2 show no obvious dependence on particle diameter. Regardless of the particle diameter used for the velocity measurement, the maximum jet velocity remain nearly constant. Contrary to the result published in [11, 3], the acoustic radiation force can be neglected in our experiments, even though the particle diameter yields $\kappa > 1$. In addition, no difference between the velocity of hollow glass spheres and silver-coated polystyrene particles of similar size can be determined. For that reason, hollow glass spheres were used to measure the fluid motion induced by the acoustic streaming, since their mean density, $1.1\ \text{g/cm}^3$, matches that of the three fluids used in our first study.

3.3 Influence of viscosity

The acoustic streaming-effect bases on the attenuation of sound waves that is dominated by two effects; heat conduction and dissipation of acoustic energy caused by the fluid's viscosity [8]. According to equation (1), the higher the viscosity the smaller the attenuation length α of the BAW, yielding a more spatially confined acoustic streaming-induced fluid motion as confirmed by comparing figure 4(a) and 4(b). In these two figures, the 2D-velocity distribution at the central z -position (regarding the aperture of the IDT) is depicted for fluid 1 and 2, see table 1. In both cases the electrical power applied to

	silver-coated polystyrene particles			hollow glass spheres
particle diameter [μm]	3.5	11	21	10
κ (in water)	0.32	1.03	1.97	0.94
\hat{v}_j [mm/s]	33.6	32.4	34.7	33.5

Table 2: Maximum jet velocity \hat{v}_j for different particles measured under same experimental conditions (fluid 1, $P_{\text{el}} = 105 \text{ mW}$).

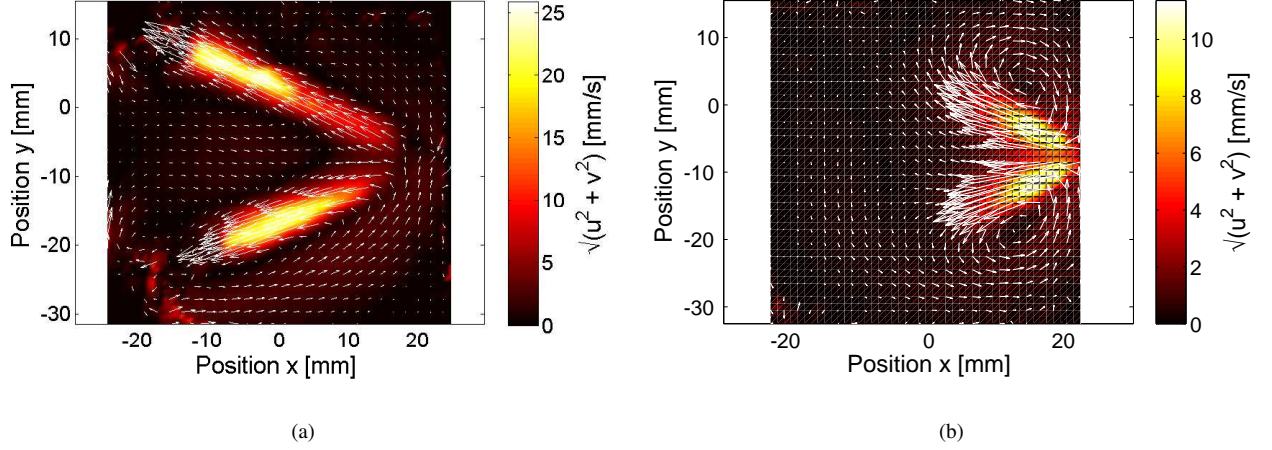


Figure 4: Measured flow velocities at the central z -position for (a) fluid 1 and (b) fluid 2 at an electrical power of $P_{\text{el}} = 70 \text{ mW}$.

the IDT amounted to $P_{\text{el}} = 70 \text{ mW}$. While the jets in water propagate almost over the entire width W of the glass cuvette, the flow induced in fluid 2 is confined to within $x > 0 \text{ mm}$ and its structure obviously exhibits much more symmetrical behavior (as generally expected). The symmetrical behavior becomes more apparent by analyzing the two jets in detail; using a two-dimensional Gaussian-model iteratively fitted to the measurement data at each x -position, as mentioned above. The determined y -position is depicted in figure 5(a) for both jets. With except for $x < 5 \text{ mm}$, the y -position increases and decreases very linearly with increasing distance to the LiNbO_3 -chip for the upper (Jet 1) and lower Jet (Jet 2), respectively. The semi-angle of about 22.7° in between both jets slightly deviates from the theoretical Rayleigh angle, which amounts to 25.6° at the speed of sound of fluid 2 listed in table 1. The extrapolated distance between both jets at the LiNbO_3 -chip amounts to approximately 1.6 mm , which means that both jets emerge above the IDT-position. This is clear, since damping of the SAW takes place directly on the mechanically loaded IDT. In figure 5(b), the beam widths in y - and z -direction of both jets

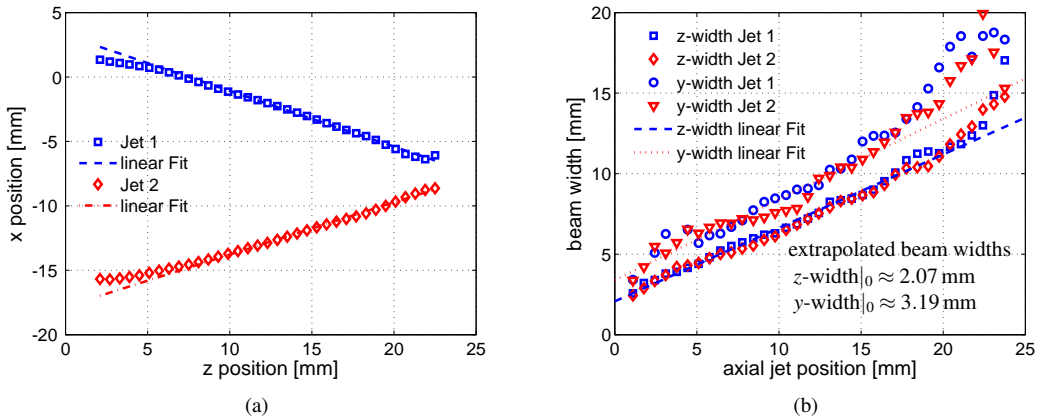


Figure 5: Determined (a) central positions and (b) widths of both jets in fluid 2.

are depicted along the axial jet position. The LiNbO₃-chip with the IDT is located at position 0. The beam width is defined by the exp(-2)-width of the 2D-Gaussian function. At first, the symmetrical behavior of both jets can be confirmed not only in y -direction, but also in z -direction. However, both jets show non-axial symmetrically behavior since width and length of the SAW, which define the size of the acoustic source of finite area, differ from each other. While the aperture of the IDT (2 mm) spatially confines the SAW in z -direction, the propagation length of the SAW along the y -direction is determined by attenuation depending on physical properties of the liquid. The size of the acoustic source can be estimated by extrapolating the beam widths towards the surface of the LiNbO₃ at position 0, assuming a linearly decreasing beam width, as illustrated in figure 5(b). By doing this, a very good agreement between the estimated width in z -direction of about 2.1 mm and the aperture of the IDT can be recognized, which also validates the measurement result. The width in y -direction, corresponding to the half-length of the SAW, can be determined to ≈ 3.2 mm. Taking the minimum distance between both jets into account, the total size of the acoustic source amounts to 2.1 mm \times 4.8 mm, approximately.

Figure 6(a) illustrates the jet velocity v_j along the axial position of Jet 1 for four different electrical power levels. Following from the no-slip condition, the jet velocity increases with increasing distance to the LiNbO₃-chip and reaches its maximum within less than 10 mm. An increase of the jet velocity magnitude with increasing electrical power level can be clearly determined. Remarkably, the position of the maximum jet velocity \hat{v}_j varies depending on the electrical power level applied, which would not be expected according to the turbulent jet model proposed by Lighthill [8]. Thus, the higher the electrical power the higher the penetration depth of the acoustically-induced fluid motion. Moreover, comparing the maximum jet velocities with those determined in water, see figure 3(b), a significant decrease of maximum velocity occurs, whereas the width of the jets does not significantly changes at the jet position of maximum velocity. Thus, more acoustic energy obviously dissipates into heat with increasing viscosity. Figure 6(b) supports this assumption. According to the measurement result, an amount of 75% of glycerin shortens the attenuation length of the BAW to the immediate vicinity of the LiNbO₃-chip, yielding a vanishingly small acoustically-induced fluid motion and, therefore, a lower heat transfer as well. As a consequence, directly at the LiNbO₃-chip a very slow buoyancy-driven convection ($< 300 \mu\text{m/s}$) arises out of a local temperature increase, inducing a counter-clockwise rotating flow inside the entire glass cuvette.

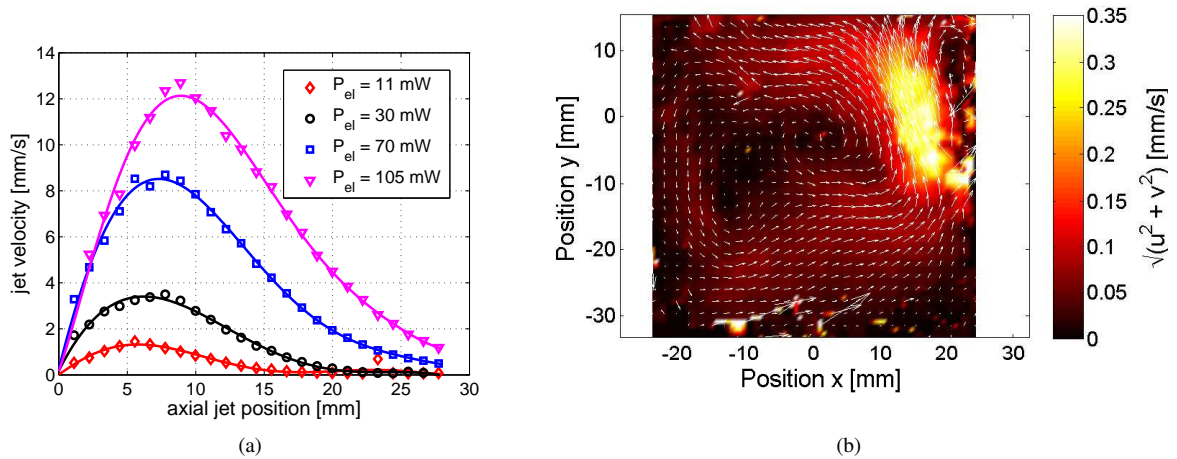


Figure 6: (a) jet velocity profiles of Jet 1 in fluid 2 for four different electrical power levels P_{el} . (b) measured flow velocities at the central z -position in fluid 3 at an electrical power of $P_{el} = 70$ mW.

4. CONCLUSION

In order to study the acoustically-induced particle motion originating from surface acoustic waves, the volumetric 3-component velocimetry (V3V) from TSI Inc. has been applied. Within its measurement volume of about 50 mm \times 50 mm \times 16 mm, which covered more than the maximum propagation volume of the bulk acoustic wave (BAW) induced in water by a SAW at a 90 μm wavelength, the position of individual particles is determined with very low uncertainty, e.g. less than 30 μm in depth. Thereby, the volumetric acoustic radiation- and streaming-induced particle motion was analyzed with high spatial resolution down to 0.06 mm³.

The three-dimensional behavior of particle motion is characterized by two bi-directional narrow jets. Starting from finite size of excitation, which is given by the size of the SAW, the two jets diverge, in water, up to 10 mm in width depending on the electrical power applied. Maximum particle velocities up to 80 mm/s were measured. A variation of velocity between silver-coated particles of significantly different size (3.5 μm and 21 μm) was not observed. In contrast to previous publications, the particle velocity remains nearly constant even though the particle size exceeds a critical value. This indicates that the acoustic radiation force can be neglected in our experiments. The reason for the difference between previous and present study has not yet been clarified. Therefore, further investigations have to be accomplished regarding the actual influence of acoustic radiation force.

The attenuation of the BAW increases with increasing viscosity. Hence, the acoustically-induced fluid motion is spatially confined depending on the fluid's viscosity. For instance, the maximum jet velocity is reached within less than 10 mm at a mixture of water-glycerin with weight percentage of 50% each. Contrary to a very simplified analytical solution, it was found: the higher the electrical power level the larger the penetration depth of the acoustically-induced fluid motion. By analyzing the fluid motion in detail, the total size of the acoustic source, given by the width and the length of the SAW, was estimated to 2.1 mm \times 4.8 mm. Starting from this finite size of acoustic excitation, the two jets diverge up to 17 mm in width much faster compared to the propagation in pure de-ionized water. In case of a mixture of water-glycerin with weight percentage of 25% and 75%, the acoustically-induced fluid motion vanishes inside the glass cuvette. Rather, fluid volume rose up very close to the LiNbO₃-chip since most of the acoustic energy dissipated into heat. This thermally-induced convection caused a counter-clockwisely rotating flow inside the glass cuvette, which is only suitable to a limited extent to mix fluids.

ACKNOWLEDGEMENT

The authors thank E. Brachmann, R. Brünig, S. Wege and A. Winkler (all IFW Dresden) for helpful comments and the support in preparation of the experiments, and A. Boomsma and D. Troolin (both TSI Inc.) for the suggestions regarding the processing of the measurement data. Funding by the German Federal Ministry of Education and Research under BMBF grant InnoProfile-Transfer 03IPT610A and by the Leibniz Association within the Joint Initiative for Research and Innovation (SAW-2014-IFW-1) is gratefully acknowledged.

References

- [1] Nian-Sheng Cheng. Formula for the viscosity of a glycerol-water mixture. *Industrial & engineering chemistry research*, 47(9):3285–3288, 2008.
- [2] Michael B Dentry, Leslie Y Yeo, and James R Friend. Frequency effects on the scale and behavior of acoustic streaming. *Physical Review E*, 89(1):013203, 2014.
- [3] Ghulam Destgeer, Byung Hang Ha, Jinsoo Park, Jin Ho Jung, Anas Alazzam, and Hyung Jin Sung. Microchannel anechoic corner for size-selective separation and medium exchange via traveling surface acoustic waves. *Analytical chemistry*, 87(9):4627–4632, 2015.
- [4] Xiaoyun Ding, Peng Li, Sz-Chin Steven Lin, Zackary S. Stratton, Nitesh Nama, Feng Guo, Daniel Slotcavage, Xiaole Mao, Jinjie Shi, Francesco Costanzo, and Tony Jun Huang. Surface acoustic wave microfluidics. *Lab Chip*, 13:3626–3649, 2013.
- [5] FAA Fergusson, EW Guptill, and AD MacDonald. Velocity of sound in glycerol. *The Journal of the Acoustical Society of America*, 26(1):67–69, 1954.
- [6] Florian Kiebert, Jörg König, Carsten Kykal, and Hagen Schmidt. Measurements of streams agitated by fluid loaded saw-devices using a volumetric 3-component measurement technique (v3v). In *Proceedings of the International Contress on Ultrasonics*. in press, 2015.
- [7] Chia-Yen Lee, Chin-Lung Chang, Yao-Nan Wang, and Lung-Ming Fu. Microfluidic mixing: a review. *International journal of molecular sciences*, 12(5):3263–3287, 2011.
- [8] Sir James Lighthill. Acoustic streaming. *Journal of Sound and Vibration*, 61(3):391 – 418, 1978.
- [9] F Pereira, M Gharib, D Dabiri, and D Modarress. Defocusing digital particle image velocimetry: a 3-component 3-dimensional dpiv measurement technique. application to bubbly flows. *Experiments in Fluids*, 29(1):S078–S084, 2000.
- [10] Mikkel Settnes and Henrik Bruus. Forces acting on a small particle in an acoustical field in a viscous fluid. *Physical Review E*, 85(1):016327, 2012.
- [11] Viktor Skowronek, Richard W Rambach, Lothar Schmid, Katharina Haase, and Thomas Franke. Particle deflection in a poly (dimethylsiloxane) microchannel using a propagating surface acoustic wave: size and frequency dependence. *Analytical chemistry*, 85(20):9955–9959, 2013.
- [12] CE Willert and M Gharib. Three-dimensional particle imaging with a single camera. *Experiments in Fluids*, 12(6):353–358, 1992.